Eur. Phys. J. D **20**, 233–242 (2002)
DOI: 10.1140/epjd/e2002-00115-2

THE EUROPEAN PHYSICAL JOURNAL D

Resonant coupling of small size-controlled lead clusters with an intense laser field

M.A. Lebeault[1,a], J. Viallon[1], J. Chevaleyre[1], C. Ellert[2], D. Normand[2], M. Schmidt[2], O. Sublemontier[2], C. Guet[3], and B. Huber[3]

[1] Laboratoire de Spectrométrie Ionique et Moléculaire, CNRS et Université Lyon I, 43 boulevard du 11 novembre 1918, 69622 Villeurbanne Cedex, France
[2] DSM/SPAM/DRECAM, CEA Saclay, bâtiment 524, 91191 Gif-sur-Yvette Cedex, France
[3] DRFMC/SI2A, CEA Grenoble, 17 rue des Martyrs, 38054 Grenoble, France

Received 18 March 2002
Published online 19 July 2002 –

Abstract. We exposed small size-controlled lead clusters with a few hundreds of atoms to laser pulses with peak intensities up to 10^{15} W cm^{-2} and durations between 60 fs to 2.5 ps. We measured kinetic energies and ionic charge of fragments as a function of the laser intensity and pulse duration. Highly charged Pb^{n+} ions up to $n = 26$ have been detected presenting kinetic energies up to 15 keV. For comparison with our experimental results, we have performed simulations of the laser coupling with a cluster-sized lead nanoplasma using a qualitative model that was initially proposed by Ditmire and co-workers at LLNL for the case of rare gas clusters. From these simulations we conclude that two mechanisms are responsible for the explosion dynamics of small lead clusters. As already observed for large rare gas clusters ($n = 10^6$), fragments with charge states below +10 are driven by Coulomb forces, whereas the higher charged fragments are accelerated by hydrodynamic forces. The latter mechanism is a direct consequence of the strong laser heating of the electron cloud in the nanoplasma arising from a plasmon-like resonance occurring at $n_e = 3n_c$. In order to obtain an optimized laser–nanoplasma coupling, our results suggest that the plasma resonance should occur at the peak intensity of the laser pulse. Due to inertial effects, even for such small-sized clusters, the observed optimum pulse duration is in the order of 1 ps which is in good agreement with our theoretical results.

PACS. 36.40.Gk Plasma and collective effects in clusters – 52.50.Jm Plasma production and heating by laser beams (laser-foil, laser-cluster, etc.)

1 Introduction

During the last decade, the study of rare gas clusters in strong and ultra-short laser fields has become a domain of active research. Since the pioneering work of the Rhodes group on hard X-ray generation using xenon and krypton clusters [1], many groups have contributed important work to progress the understanding of the cluster response in particular on cluster heating mechanisms and the explosion dynamics of nanometer-scaled clusters [2–4]. These preliminary studies have evidenced an explosion process leading to atoms brought to very high charge states as compared to similar experiments on isolated atoms or molecules. However most of the studies have been realized with large rare gas clusters (10^5–10^6 atoms per cluster) [4,5]. The interaction between the strong laser intensity and such clusters is revealed by an important production of electrons, mono atomic ions and X-ray emission. In particular Ditmire has detected Xe^{40+} ions with a kinetic energy up to 1 MeV [6]. The electron emission has been measured in a keV magnitude by Shao *et al.* [7] in the explosion of xenon clusters. Finally the X-ray emission reached 5 keV in the Thompson *et al.* [7] experiment where rare gas clusters were irradiated by a 10^{19} W cm^{-2} field intensity. This last phenomenon signs the presence of an internal recombination in atomic internal shells which involves very high ionization energy. In all the beyond experiments on clusters, the very high energy detected demonstrates that the energy absorption process is quite different from processes involved in molecules or atoms submitted to similar irradiation [8,9].

In parallel several theoretical approaches have been introduced to explain these observations on clusters. Rhodes and co-workers [2] used a model based on collective electron motion. Indeed the electrons oscillations driven by the laser field induce electrons ions collisions which enhance the ionization inside the cluster. Rose-Petruck *et al.* [10] introduced an "ionization ignition model" where, for a given atom, ionization is driven by the

[a] e-mail: lebeault@lasim.univ-lyon1.fr

combined fields of the laser, the other ions and the electrons. On the other hand, to explain the high ionic charge states [11], their high kinetic energy [6], the high electronic temperature [7] and the X-ray emission in the keV range Ditmire *et al.* [12] proposed an hydrodynamic model in which ions are ionized through impact of hot electrons. Indeed, they showed that, after the departure of the first electrons extracted by field ionization, an important rate of electrons is trapped in the coulomb potential of the highly charged ions. They formed a nearly free electron gas whose density, due to the cluster expansion, evolves and reaches such a value that its plasmon frequency comes into resonance with the laser frequency. Then clusters absorb a huge amount of energy from the laser which leads to their explosion in highly charged mono atomic fragments. The important role of the electrons cloud underlined by Ditmire raises the issue of the influence of an already existing free electron gas, as it occurs in metallic clusters. Indeed, such clusters represent the best target to investigate collective response of an electronic cloud irradiated by a laser field. Many experiments have been carried out with lower laser intensity. In particular Bréchignac *et al.* [13,14] have demonstrated that the valence electrons participate in the giant dipole resonance with a laser field intensity below 10^5 W cm^{-2}. The Haberland group using a 10^{13} W cm^{-2} field has shown some photo fragmentation in sodium cluster Na_{93}^+ [15]. Compared to nanosecond experiment with the same energy deposited the ionization leads to ionic fragments Na_n^+ instead of a Na_n^{q+} with $1 < q < 3$ observed in femtosecond experiments. They interpreted this result using a multiple excitation process of the plasmon resonance followed by an auto ionization. The first observation of a Coulomb explosion of metal clusters in intense laser fields concerned mercury clusters in Lang *et al.* [16] experiments. Increasing progressively the laser intensity from 10^{11} W cm^{-2} to 10^{13} W cm^{-2} they observed ionic fragments produced in the charge range: $q = 1, 2$ for 10^{11} W cm^{-2} up to $q = 5$ using 10^{13} W cm^{-2}. Moreover the recent experiments realized in the Meiwes-Broer group [17–19] on platinum clusters irradiated by a 10^{16} W cm^{-2} field intensity have revealed a pulse duration influence on the maximum charge value (+20) observed on the mono atomic ionic fragments Pt^{z+} detected. To interpret such results they proposed to take into account the plasmon frequency evolution of a charged cluster in expansion during the laser absorption. For metal clusters some time dependent density functional calculation (TDFT) on sodium clusters Na_{93}^+ at medium laser intensities of 10^{11} W cm^{-2} by Calvayrac [20] have shown that with pulses in the vicinity of the plasmon resonance enormous field amplification could be achieved. It results in a charged cluster Na_{93}^{10+} which is then submitted to coulomb repulsion. More recently Doppner *et al.* [21] have proposed some experimental investigations on Pb and Pt clusters with variable pulse widths and, with the pump&probe technique. They conclude that both approaches support the picture according to which, after an initial charging, the clusters expand due to Coulomb forces. Indeed this expansion is accompanied by a reduction of the electron density and at the same time by an increase of the optical sensitivity.

In this work we used ionic spectrometry to analyze the response of lead clusters exposed to an intense laser field of 10^{15} W cm^{-2}. The knowledge of the kinetic energy of the ionic fragments leads to information on the explosion mechanism. These results are interpreted using the qualitative "nanoplasma" model developed by Ditmire *et al.* [12]. Furthermore, an experimental study of the influence of the irradiation conditions (pulse duration and laser intensity) on the ionic signal is compared to simulations on lead clusters under the same conditions.

2 Experimental details

2.1 Set up description

The experimental setup schematically drawn in Figure 1a consists on a cluster source, a femtosecond laser for the cluster excitation, and a mass spectrometry system. To produce lead clusters we used a laser vaporization source [22] using a 532 nm Nd:YAG focused on a 6 mm rotary lead rod. A pulsed solenoid valve is used to deliver a 300 μs pulse of argon carrier gas which cools down the laser induced plasma. The nucleation is achieved by expansion of the mixed gas through a 1 mm diameter conical nozzle. The backing pressure for the carrier gas was kept between 7 to 9 bars. We have chosen argon as carrier gas to obtain a mean cluster size of 250 atoms as shown in Figure 1b. The pulsed cluster beam is then skimmed before entering the analysis chamber where the operating pressure is maintained below 10^{-7} torr. To ensure that only neutral clusters enter the interaction zone, ions produced directly by the source are deflected by an electrostatic field placed after the skimmer. Remaining neutral species enter the extraction region of the Wiley-McLaren type time-of-flight mass spectrometer (TOF-MS) where they interact with the terawatt femtosecond laser beam of the LUCA facility at CEA-Saclay operating at 20 Hz. The nominal pulse duration is 70 fs but by varying the compressor position, we could increase continuously the pulse duration up to 2.5 ps. The pulses are focused with a $f = 50$ cm lens into the cluster beam at about 50 cm downstream from the nozzle. The lens is chosen to avoid lengthening of the ultra-short pulses. The resulting spot is in the order of 30 μm which gives maximum possible peak intensity of 3×10^{16} W cm^{-2} with pulse energies of 35 mJ, 70 fs pulse duration and 790 nm wavelength. The laser-jet interaction zone is located in the center of a 6 cm long extraction zone of the linear two stages TOFMS (Fig. 1a). The ions were extracted by an electric field of 360 V cm^{-1}, and are post accelerated in a second region of 1 cm length by a 2 kV voltage towards a 60 cm long field free drift region and then detected by a Philips XP1600 secondary electron multiplier.

As shown in Figure 1, another 9 cm long drift tube has been placed on the opposite side of the TOF-MS to realize a potential barrier spectrometer (PBS) Both spectrometers share the same entering zone that are labeled

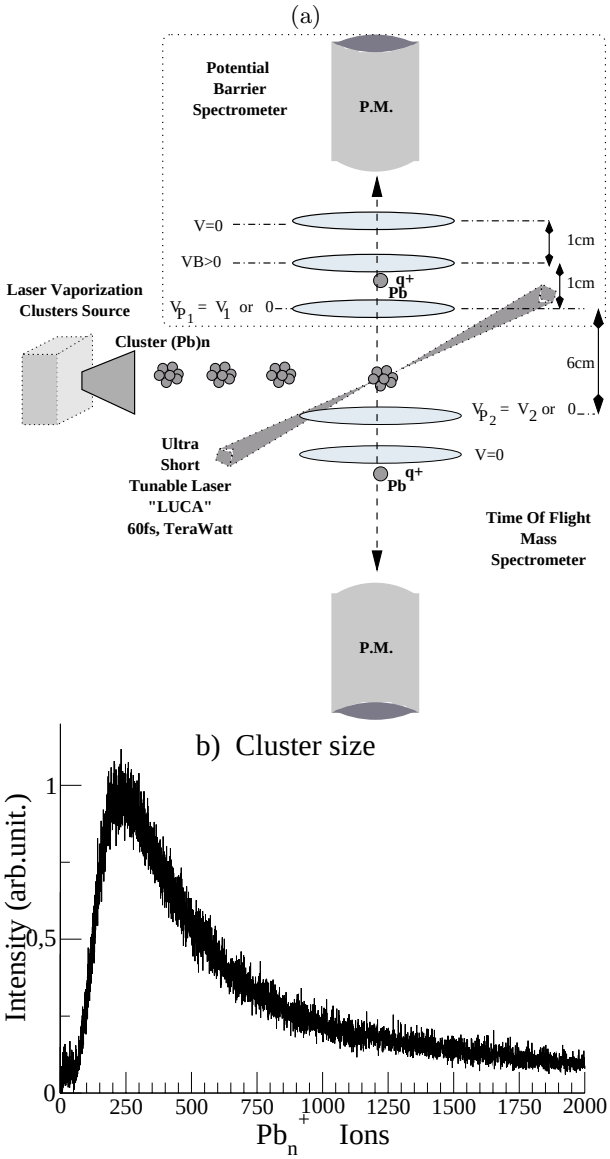

Fig. 1. (a) Experimental setup: composed with a clusters sources, the Luca Laser beam, the PB spectrometer and the time of flight mass spectrometer. V_{P_1} and V_{P_2} potentials are set to zero when PBS is operating and set respectively to positive values V_1 and V_2 (with $V_1 > V_2$) when TOFMS is operating. (b) We show a mass spectrum of the cluster size distribution reached with our cluster vaporization source.

extraction zone of the TOF-MS. The charge state distribution and kinetic energies of ions produced by the interaction of the laser pulse with the clusters are determined by measuring the TOF of those emitted in direction of the PBS. Our PBS device consists of three closely spaced grids placed in parallel along the drift tube (see Fig. 1a). Whereas the front and the back grid were grounded, the middle grid is set to positive potential V_B which introduces a potential barrier for the Pb^{q+} ions with energy below qV_B without significantly altering the overall TOF of more energetic ions.

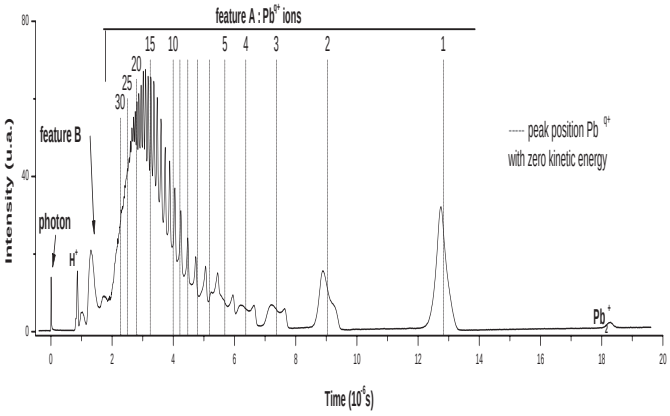

Fig. 2. Typical TOF mass spectrum: spectrum of Pb^{q+} ions obtained by irradiation of lead clusters for an average of 1 000 efficient shots under the laser conditions followed; 760 fs laser pulse duration at 3×10^{15} W cm^{-2} for $\lambda = 790$ nm.

2.2 Experimental methods : mass assignment and determination of the kinetic energy

Using the TOF-MS, we were able to discriminate ions both according to their charge-to-mass ratio (q/m) and their kinetic energy. A typical spectrum is shown in Figure 2. For a given (q/m) we observe a broad peak that can be splitted into two separate peaks for larger charge. The interpretation of this feature is straightforward since it indicates an initial kinetic energy of the corresponding fragments. Indeed during the explosion resulting from the laser cluster interaction, high energetic mono atomic ions are isotropically emitted. Due to the restricted detection angle of the TOF-MS, two classes of ions are detected, *i.e.* the so-called forward ions flying directly to the detector and the backward ions that are emitted in the opposite direction and then reflected by the repeller grid. A characteristic difference of the TOF, Δt, is measured between forward and backward ions. Using the geometrical and electrostatic parameters of our TOF-MS it comes the initial kinetic energy E_k of a fragment ion with charge q and mass m from the following expression [23]:

$$E_k(\text{eV}) = 1.2 \times 10^{-7} \frac{\left[\Delta t(\text{ns}) \times qE_1(\text{V cm}^{-1}\right]^2}{m(\text{u.a.})} \qquad (1)$$

where E_1 is the extraction field. As an example, Figure 2 shows an experimental TOF spectrum obtained after interaction of Pb_n cluster with 760 fs pulse duration and a peak intensity of 9×10^{14} W cm^{-2}. We observe that forward and backward ions with $q = 1$ to 5 are fully resolved and can be analyzed with equation (1).

We want to stress that using the classic TOF-MS technique is however not possible to discriminate different ion species with identical or at least similar q/m ratios. This may arise in our spectra since two different species are present in our jet namely argon and lead. In order to overcome this difficulty we have applied the PBS technique which allows to discriminate the low kinetic energy argon ions from the Pb^{q+} fragment ions since these ions

present much higher kinetic energies. Indeed by a applying a positive potential $0 \leq V_B \leq 3$ kV Ar^{q+} ions are systematically blocked, since the kinetic energy of fastest one Ar^{8+} never exceeded several tens eV and allows to detect Pb^{q+} fragments with kinetic energy beyond qV_B. Their kinetic energy, depending on their arrival time on the detector, is established to be:

$$E_k = \frac{1}{2} m \left(\frac{d}{t}\right)^2 \quad (2)$$

where $d = 89.5$ mm is the total free flight distance. Thus, for a given kinetic energy E_k two consecutive experimental values of potential barrier V_{B_1} and V_{B_2} define ion signals with a kinetic energy beyond qV_{B_1} but below qV_{B_2}. For each curve at a given E_k it becomes easy to construct the response signal intensities as a function of V_B. As V_B is related to the ionic charge according to:

$$\frac{E_k}{V_{B_2}} < q < \frac{E_k}{V_{B_1}} \quad (3)$$

where the intensity I_{E_k} is a function of $q_{lim} = E_k/V_B$, and q_{lim} is the limit charge state value. In a final step, by derivation of this last curve, we are able to obtain the ions charge distribution for different kinetic energies.

3 Results and discussion

The goal of the present study is to analyze the explosion dynamics of metallic cluster into fast mono atomic ionic fragments. We have chosen a systematic approach in which we have varied either the laser pulse energy or the laser pulse duration. Before describing the results of our systematic study, we show in Figure 2 a typical TOF-MS Pb^{q+} spectrum obtained after interaction of Pb_n clusters ($n = 250$) with 760 fs laser pulses at 3×10^{15} W cm^{-2}. The spectrum is the result of an average over 1 000 *efficient* laser-cluster interactions. Indeed, during our experiments we have observed that only a fraction of laser shots yield energetic cluster explosion characterized by fast and highly ionized fragments. This important instability in the recorded ions signal cannot be attributed to the femtosecond laser pulse whom energetic stability is in the order of 2%. We must consider the number of clusters irradiated by the LUCA laser pulse as responsible for this large instability. While the cluster size distribution is stable over the global volume of the cluster burst, it can vary considerably in the very small volume irradiated in the waist (30 μm diameter) of the LUCA laser spot. Internal shell excitation and ionization lead simultaneously to both highly charged ions and soft and hard X-ray photons. Thus, only those spectra presenting such a photon signal are called *efficient* spectra. For this reason, we have triggered the ion detection device on this signal using the smart trigger option of our digital oscilloscope (Tektronix TDS 520C). All TOF spectra in this paper have been recorded as an average over 1 000 efficient shots.

In the spectrum presented in Figure 2 we can assign several features namely two groups of ionic Pb fragments labeled feature A and feature B, a photon signal at TOF = 0 μs, as well as a proton signal at TOF = 1 μs; and the Pb-dimer signal at TOF = 18.2 μs. First of all, it must be noticed that, except the very weak signal recorded on Pb_2^+, no other cluster signal is detected. Let us first discuss the major feature (*i.e.* feature A) which is located between 2.2 and 14 μs. The highest resolved charge state in feature A that can be identified is Pb^{26+}. Nevertheless, in its unresolved left wing, forward ionic fragments with charge states higher than 30+ are probably present. For more clarity we indicate the TOF positions for zero kinetic energy Pb^{q+} ions with $q = 1$, ..., 30 in Figure 2. Under some comparable experimental conditions, we have also applied the PBS technique in order to confirm the energy values deduced from the TOF spectrum in Figure 2. The analysed PBS spectra are plotted in Figure 4, where we have determined for several kinetic energy value the lead ion charge state distribution. As for the TOF-MS results, Pb^{q+} ions with charge states up to 30+ and kinetic energies up to 15 keV are detected. Interestingly, feature B, located at TOF around 1.6 μs, appears solely under conditions where the highest charge states in feature A are observed. We have carefully checked that the only origin of feature B is the presence of very fast Pb^{q+} fragment ions. Assuming the presence of Pb^{30+} ions, we can deduce a kinetic energy of 200 keV. This observation is quite analog to that described in earlier studies on xenon clusters [5] and agree with the conclusion of this work that feature B can be attributed to the fastest ions with the highest charge states Xe^{q+}. Finally, using our PBS device we have observed no change of this features even with the highest potential barrier ($U_B = 3$ kV). The above considerations strongly suggest that quite different acceleration mechanisms must be involved to explain the presence of features A and B.

To interpret the above results, we have plotted in Figure 3 the fragment initial kinetic energies *versus* their charge obtained for the optimum laser conditions. Those conditions are defined by the observation of the highest charge state (26+) on feature A ions. Two regimes of q dependence *versus* the kinetic energy appear. The initial kinetic energies behavior of ions with $q = 1$ to 10 can be described with:

$$E_k(q)[\text{eV}] = \alpha_c q^2 \quad \text{assuming} \quad \alpha_c = 35 \text{ eV}/q^2, \quad (4)$$

whereas for highest charge states a linear dependence is found:

$$E_k(q)[\text{eV}] = \alpha_h q \quad \text{assuming} \quad \alpha_h = 725 \text{ eV}/q. \quad (5)$$

Similarly to the approach of Lezius *et al.* [23], we attribute these observations to two distinct explosion mechanisms. Ions with small charge states are ejected from the cluster by Coulomb repulsion. Indeed, a charged sphere model where a Pb^{q+} ion is surrounded by ions with same charge states leads to an energy pattern $E_k(q) \propto q^2$. Concerning ions with higher charge states (>10), the linear dependence of the kinetic energies on their charge states

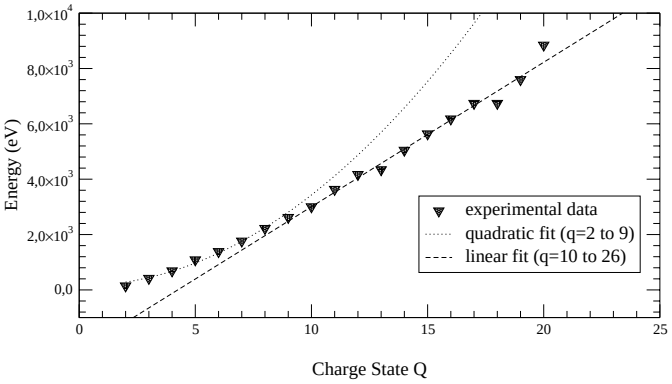

Fig. 3. Pb^{q+} kinetic energy *versus* charge state behaviors: Ionic fragments analysis of Pb_{250} exposed in an intense laser field; 760 fs pulse duration at 3×10^{15} W cm^{-2} for $\lambda = 790$ nm.

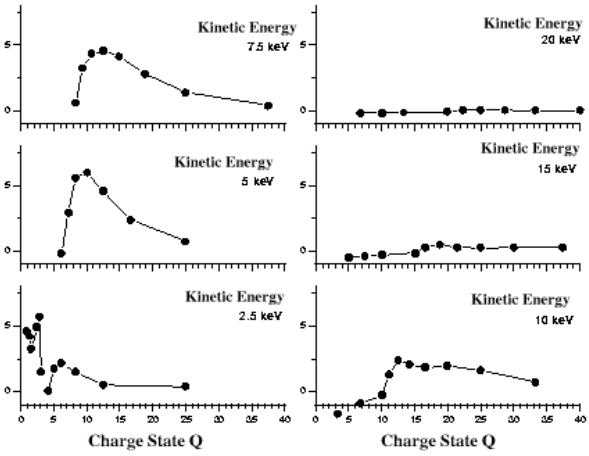

Fig. 4. Charge states and energies determined with the potential barrier spectrometry techniques. Ionic fragments detected of Pb_{250} exposed in an intense laser field; 760 fs pulse duration at 2.5×10^{15} W cm^{-2} for $\lambda = 790$ nm.

is attributed to a hydrodynamic expansion of the cluster. This expansion leads to a linear kinetic energy dependence on q for the Pb ions $E_{\rm k}(q)[\rm eV] = \alpha_{\rm h} q$. The expression $\alpha_{\rm h} = \gamma k T_{\rm e}/2$ is evaluated by fitting the energy $E_{\rm k}$ which allows to deduce the electronic temperature $T_{\rm e}$ at the instant when explosion starts [23]. In order to qualitatively interpret such kinetic energy behavior we adapted the nanoplasma model, initially developed by Ditmire [12], to metallic clusters. This model supports the assumption that a cluster irradiated with an ultra short high intensity laser pulse is considered as a small spherical plasma formed by ions within a hot electron cloud, the whole behaves in a constant expansion. Indeed, this model evaluates the intra-cluster electric field by assuming an interaction between a metallic sphere and a plan wave. In brief, this model uses hydrodynamics to describe the nanoplasma as a fluid in expansion including tunneling ionization, plasma collision mechanisms to deposit energy by inverse bremsstrahlung heating, as well as electron

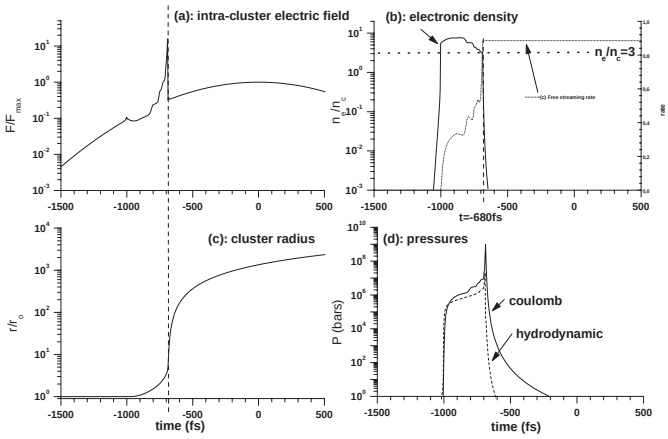

Fig. 5. Nanoplasma parameters calculated with the Ditmire model for Pb_{250} with the laser conditions; 760 fs laser pulse duration at 10^{15} W cm^{-2} for $\lambda = 790$ nm. Time origin corresponds to the maximum intensity of the femtosecond laser pulse, the long vertical dash line indicates the major resonance.

ion collisional ionization. Despite its relative simplicity, the nanoplasma model allows us to calculate the pertinent cluster parameters such as electronic temperature and density, and cluster radius as a function of time. A simulation performed on a Pb_{250} cluster irradiated by a 760 fs laser pulse with a peak intensity of 10^{15} W cm^{-2} is shown in Figure 5. In particular, the figure shows the time evolution of the intra-cluster electric field (Fig. 5a), the electronic density (Fig. 5b), the cluster radius (Fig. 5c), and the nanoplasma pressure (Fig. 5d). For all these figures (Figs. 5a–5d), the crucial instant is defined as a strong resonance effect at around -680 fs indicated by a vertical dotted line. This resonance induces a sudden increase of the intra-cluster electric field that is at least two orders of magnitudes higher than the external laser field. The beginning of cluster explosion, when the cluster radius dramatically enhances, is strongly linked to this resonance which is due to the massive loss of the hottest electrons thereby creating an important positive excess charge. At the resonance, the nanoplasma pressure is very important but vanishes rapidly on a short time scale. From a more formal point of view, using the Drude model [24] to modelize the response of neutral nanoplasma irradiated with the laser pulse allows the use of the dipole approximation since applied wavelength $\lambda = 790$ nm is larger than the 1.22 nm Pb_{250} cluster radius. The intra-cluster electric field due to applied electric field E_0 and the free electron gas oscillations is evaluated by Bertier [25] as follows $E_{\rm int} = (3/|\epsilon + 2|)E_0$, where ϵ is the Drude model plasma dielectric function. It comes that the intra-cluster electric field depends on the ratio $(n_{\rm e}/n_{\rm c})$ and reaches its maximum at the resonance condition $(n_{\rm e}/n_{\rm c}) = 3$. In this expression $n_{\rm e}$ represents the electronic density of the nanoplasma and $n_{\rm c}$ the critical density defined as the electronic density for which the free electron gas oscillations is equal to the frequency of the applied wave. This situation is reached twice during the pulse duration. Whereas the first resonance is quite inefficient in terms of laser energy

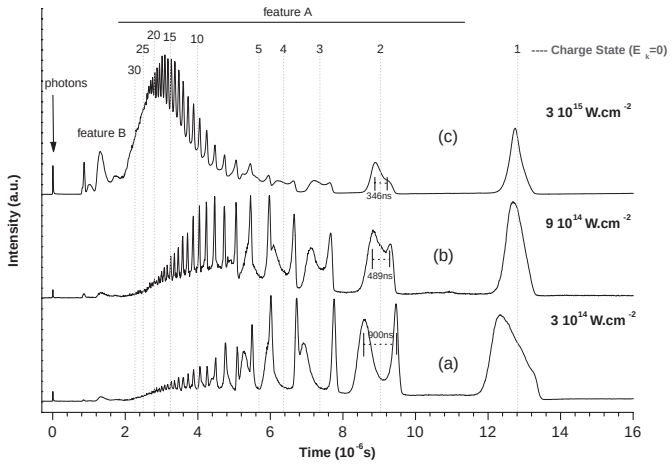

Fig. 6. Time of flight mass spectra: signal curves obtained for three fluence values at a laser pulse width constant 760 fs.

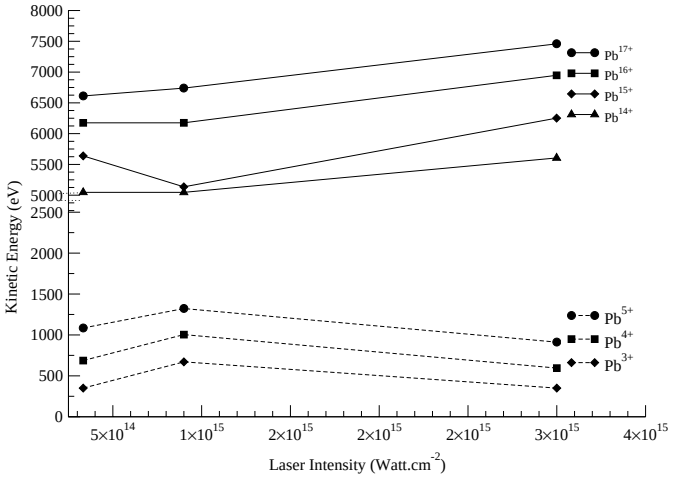

Fig. 7. Kinetic energy of several ionic fragment Pb^{q+} obtained under three fluence values with a laser pulse width constant 760 fs.

absorption since the electron cloud is still too small, the main energy absorption occurs at the second resonance. The nanoplasma model includes both the description of the hydrodynamic and electrostatic pressures. Figure 5d indicates that the respective contributions of these mechanisms are slightly different which might explain the two classes of cluster fragments (see above).

In order to understand the characteristic energy evolution as a function of the fragment ion charge q, we present in the following paragraph a systematic set of experimental results. This set of experimental results, obtained for different laser intensities and pulse duration, is then compared to our simulations using the nanoplasma model.

3.1 Energy dependence

We have performed our systematic experimental study of the lead cluster explosion dynamics with an average cluster size of 250 atoms. At a working wavelength of 790 nm and a fixed pulse duration at 760 fs, we have varied the laser peak intensity. Three typical TOF-MS spectra are presented in Figure 6 obtained at 3×10^{15} W cm^{-2} (a), 9×10^{14} W cm^{-2} (b) and 3×10^{14} W cm^{-2} (c). Already at a first glance, we can remark that strongly increasing fragment charge states are produced with increasing intensities and in parallel the abundance of the lower charge states ($q \leq 5$) strongly decreases. Concerning feature B and the photon signal a very similar behavior is observed. Indeed, these three observables appear closely connected with the energy absorption in lead nanoplasma.

In contrast, for fragment with $q \leq 5$, we observe a decrease of the kinetic energy when increasing the laser intensity. This effect is underlined in Figure 7 where one has plotted the ions kinetic energy *versus* the laser intensity for several Pb^{q+}. The nanoplasma model is perfectly relevant to interpret this quite counterintuitive result. Let us refer to Figure 8 that shows the simulated evolution of the cluster radius for different laser intensities. After the departure of the first electrons, the nanoplasma begins to

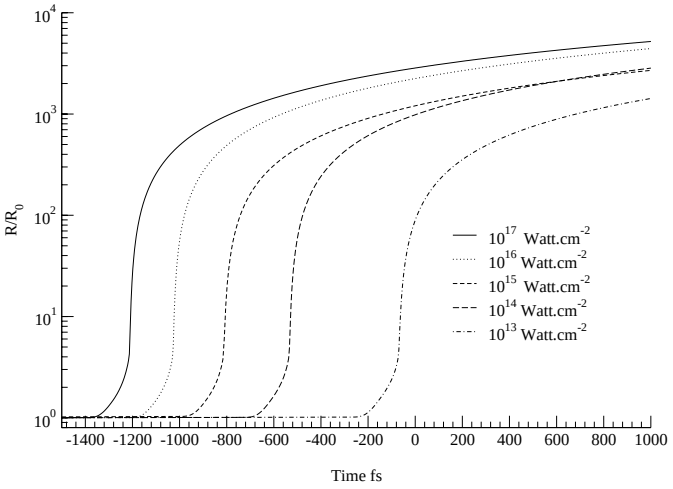

Fig. 8. Simulations results: evolution of the cluster radius (Pb_{250}) for different laser fluences during a constant pulse duration.

expand because it is submitted to Coulomb forces leading to a Coulomb pressure. Briefly, the cluster is assimilated to a conductive charged sphere, (radius r, charge Q) the coulomb pressure defined as the ratio of the conductor energy over the sphere volume is evaluated as follows $P_{\text{Coulomb}} = 3Q^2/(2(4\pi)^2\epsilon_0 r^4)$. For increasing intensities the explosion is more and more violent and occurs at earlier stages but always starting at some characteristic threshold intensity for a given fragment charge state. We can reasonably assume that the smallest charge states (*e.g.* $q = 2$ in Fig. 6) originates from the cluster periphery and are ejected *via* Coulomb repulsion early in the pulse. Therefore, the fragment kinetic energy results in a $1/r^4$ dependence [12] whereas the characteristic intensity threshold is reached earlier in more intense pulses. This implies that fragments $q \leq 5$ present decreasing energies for increasing laser intensities since they are emitted from increasing cluster radii.

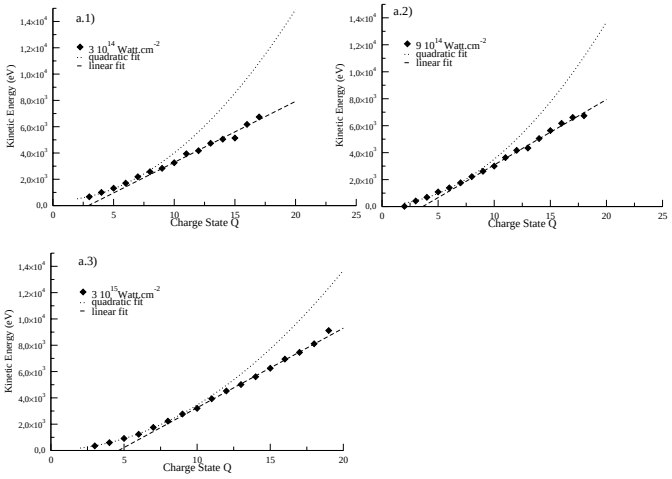

Fig. 9. Experimental kinetic energy *versus* charge state; each graph correspond to Figure 6 spectra obtained at different laser fluence and a constant laser pulse duration 760 fs.

On the other hand the opposite behavior of the higher charge states $q \geq 6$ can be explained in the same way when assuming that these ions are created in the nanoplasma core at a later stage of the laser pulse. However, these ions are driven by the hydrodynamic pressure of electron cloud which reaches the highest temperatures at the nanoplasma resonance ($n_e/n_c = 3$).

Moreover we have plotted in Figure 9 the kinetic energy *versus* charge state of all the feature A ions from Figure 6. Examination of Figure 9 demonstrates that always two acceleration regimes exist namely a linear and quadratic energy dependence on charge state Q whatever the intensity is deposited we always observed two classes of Q range. One class concerns the [2–9] Q range and reflects a coulomb repulsion behavior, the other Q range [10–20] reveals an hydrodynamic expansion of Pb^{q+} fragments. The analysis of the linear behavior allows us to connect the laser intensity, with the energy absorbed by the cluster *via* the electronic temperature T_e reach at the explosion time. The electronic temperature values are listed in Table 1, and vary with respect to the laser fluence.

3.2 Pulse duration dependence

For this experiment we have submitted lead clusters of an average size of 250 atoms per cluster into the LUCA laser beam characterized by a 790 nm wavelength, a 9×10^{14} W cm^{-2} constant intensity and a pulse duration value which has been varied from 208 fs to 2 490 fs.

Mass spectra analysis of these ionic fragments are shown in Figure 10, we have also plotted in Figure 11 different Pb^{q+} kinetic energy curves to underlined the evolution of the fragment depending on the laser pulse duration. The investigation of these spectra, where the laser pulse duration increases and the intensity is constant, points out the giant resonance role regarding the clusters energy absorbed. This effect is illustrated in Figure 12, where the maximum ions charge state observed in Figure 10 spectra

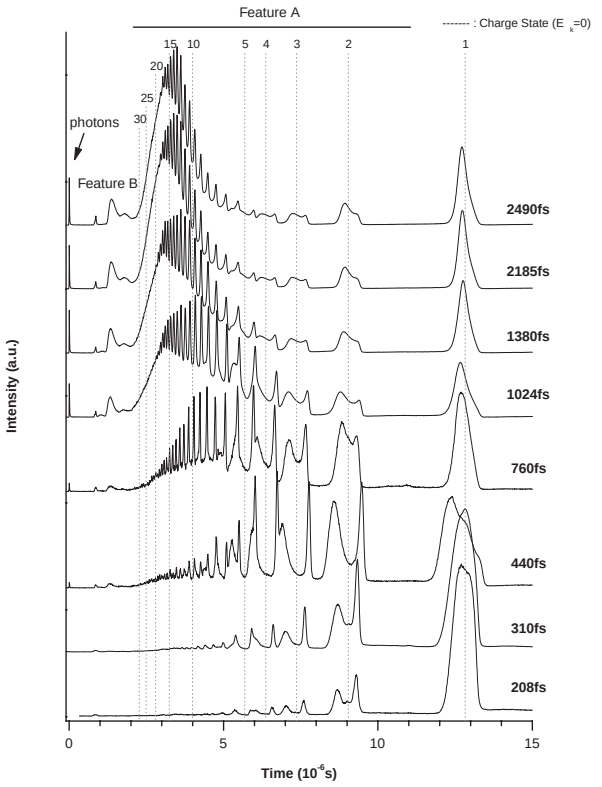

Fig. 10. Time of flight mass spectra obtained at different pulse durations under a constant laser fluence of 9×10^{14} W cm^{-2}.

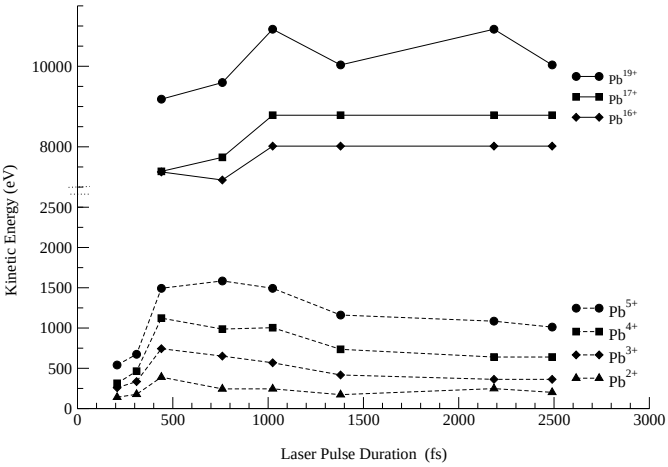

Fig. 11. Kinetic energy of several ionic fragment Pb^{q+} obtained at different pulse durations under a constant laser fluence of 9×10^{14} W cm^{-2}.

is plotted *versus* the laser pulse duration. Let us note that for those spectra, we can consider the total number of ions per spectrum constant and determined by the mean number of atoms in clusters irradiated along the 1 000 laser shots average. As a consequence, the highest charge state distribution is closely related to the absorbed energy. Figure 12 shows that absorbed energy increases rapidly up to 1 000 fs laser pulse duration, and then reaches a quasi-constant value. This behavior is in close connection with the synchronism between the laser pulse and the giant

Table 1. Fitted parameters obtained with two kinds of kinetic energy *versus* q behavior. The number in parenthesis represents the error.

Intensity	Δt	Quadratic function			Linear function			Temp.
W/cm^2	fs	$AQ^2 + B$ (Q$\in$ 2−9)			$aQ + b$ (Q$\in$ 10−20)			eV
		A	B	χ^2	a	b	χ^2	
3×10^{14}	760	36.4 ± (2.6)	369 ± (62)	1.2/4	464 ± (48)	−1359 ± (635)	2.6/8	560 ± (60)
9×10^{14}	208	18 ± (10)	−69 ± (290)	2/5				
9×10^{14}	310	16 ± (15)	187 ± (150)	2/5	287 ± (69)	−1338 ± (806)	1.5/4	344 ± (83)
9×10^{14}	440	36.3 ± (10.8)	483 ± (290)	0.25/5	588 ± (152)	−2 392 ± (2 171)	0.35/8	705 ± (182)
9×10^{14}	760	32.8 ± (9.3)	150 ± (228)	0.13/6	522 ± (126)	−2 216 ± (1 850)	0.29/9	626 ± (151)
9×10^{14}	1 024	47.1 ± (11.1)	194 ± (270)	0.16/7	715 ± (22)	−2 917 ± (2 055)	0.33/11	857 ± (163)
9×10^{14}	1 380	42.8 ± (10.2)	48 ± (235)	0.09/5	706 ± (122)	−3 151 ± (1 874)	0.37/11	847 ± (146)
9×10^{14}	2 185	41.2 ± (9.8)	−5 ± (222)	0.03/7	773 ± (132)	−4 050 ± (1 980)	0.26/11	927 ± (160)
9×10^{14}	2 490	40 ± (9)	8 ± (222)	0.05/7	744 ± (143)	−3 802 ± (2 087)	0.19/10	893 ± (172)
3×10^{15}	760	34 ± (2)	45 ± (44)	0.2/5	605 ± (42)	−2 802 ± (565)	0.2/7	726 ± (50)

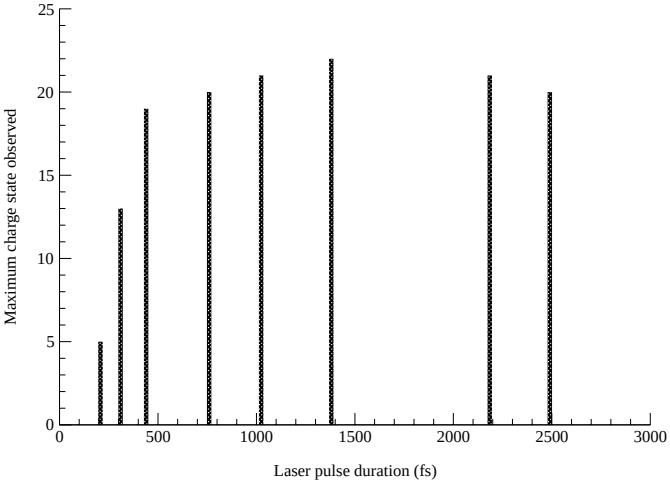

Fig. 12. Experimental maximum charge state *versus* the laser pulse duration obtained from the feature A analysis for experiments realized under a constant laser fluence of 9×10^{14} W cm^{-2}.

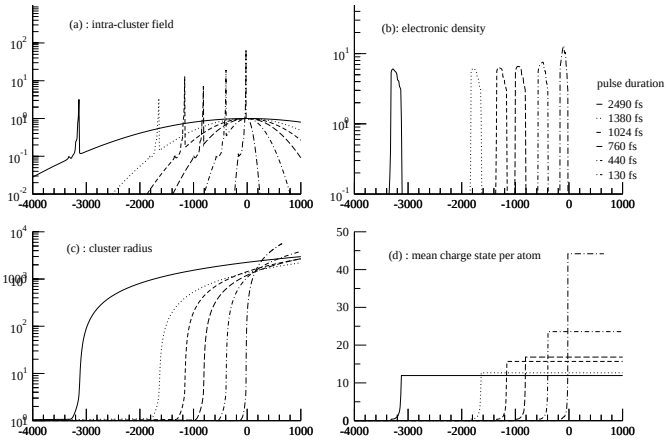

Fig. 13. Simulations obtained for different pulse duration. Performed on Pb_{250} under a constant intensity 10^{15} W cm^{-2}.

resonance occurring between the electron cloud and the laser field. As long as the cluster is irradiated with a very short pulse duration, the resonance condition $n_e/n_c = 3$ is reached after the maximum of the pulse, so the intra-cluster field increase is not sufficient to reach some high ionization degrees. It does exist an optimal pulse duration which provides an efficient overlap to reach charge state close to Pb^{30+} and obtained in Figure 2 spectrum with $I = 3 \times 10^{15}$ W cm^{-2} 790 nm wavelength and 760 fs pulse duration. This kind of resonance has already been observed and this optimal pulse duration value is evaluated on xenon cluster at 1 000 fs by Zweiback *et al.* [26] and on Pt_n clusters by Köller *et al.* at 800 fs [18]. The occurrence of this resonance gives a clear explanation of the apparently contrary result observed *via* the ions kinetic energy *versus* their charge state behavior. Indeed Figure 10 spectra obtained under laser pulse duration below 440 fs show a lack of high charge state ions which means that only few energy is absorbed by the cluster. Beyond 760 fs pulse duration, the presence of high charge state ions reveals a sudden increase of cluster energy absorbed. In this case, the kinetic energy of low charge state ions, shown in Figure 11, evolves in an opposite way: it decreases when laser intensity increases. According to the nano-plasma results, shown in Figure 13c, the cluster size increases of two orders of magnitude. As the pulse duration increases one verifies that the kinetic energy low charge states decreases. This behavior modification of low charge states ejected ions ($q < 8$) is connected to the fast increase of cluster size. Indeed ions with low charge state close to the cluster periphery are ejected by coulomb repulsion following a $(1/r^4)$ law. For those long pulse durations the main effect is fundamentally connected to the energy absorption when the resonance condition is reached. In fact in this pulse duration range, a pulse duration increase does not lead to an increase of the absorbed energy. Indeed from the linear behavior observed for ions with q ranging from 10 to 20 in all Figures 10 spectra and illustrated in Figure 14 we can deduce the electronic temperature at

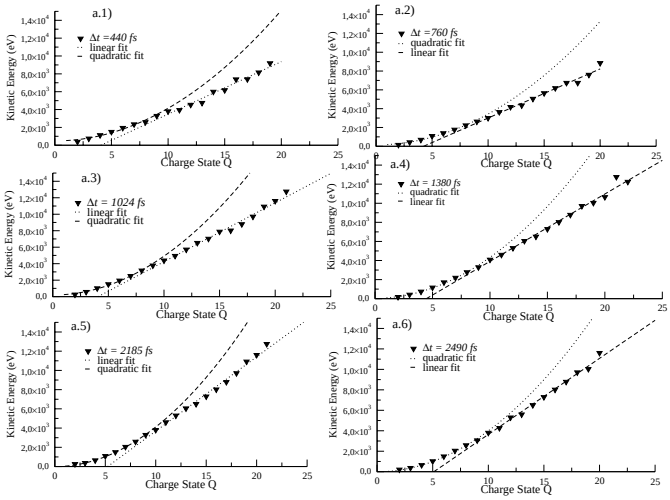

Fig. 14. Experimental kinetic energy *versus* charge state; each graph correspond to Figure 10 spectra obtained at different laser pulse duration and a constant laser fluence 9×10^{14} W cm^{-2}.

the explosion time. These temperatures are listed in Table 1 and confirm this resonance dependence effect since we observe a T_e increase from 600 eV to 950 eV around the 1 000 fs laser pulse duration. With regard to the cluster size distribution produced with the laser vaporization source and because spectra have been recorded for an average of 1 000 LUCA laser shots, ions detected come from the explosion of several size clusters. As a consequence we have shown that this sudden increase around [760–1 000] fs occurred depending on the absorbed energy value for all cluster size. Indeed if that wasn't the case this particular effect would be smoothed in the laser pulse width range we used, and the absorbed energy would increase regularly.

Experimental results as well as simulations demonstrated that electron cloud is present at least during 800 fs to enhance energy absorption. In order to qualitatively characterize this electron cloud we have fitted experimental kinetic energy values with a quadratic function for the smallest charge states and a linear one for the highest charge states. In Figure 14 we have reported the kinetic energy *versus* the charge state of ionic Pb^{q+} fragments observed in feature A from spectra obtained in the conditions of varying the pulse duration. We have also listed the set of fitted parameters obtained with the two kinds of laser conditions in Table 1. The first observation arising from this study concerns the stability of the parabolic behavior. It is related to same range from $q = 2$ to $q = 9$ whatever the laser condition. With regard to the error bars we obtained similar fitted parameters of the kinetic energy dependence on charge state. From these fitted results, due to the laser pulse duration and energy independence on the mechanism involved here, it comes that our assumption concerning the ions fragment charge state below 10 is relevant. Those ionic fragments are generated by coulomb repulsion between cluster ions at the beginning of the laser pulse, when the tunneling ionization is very efficient, and emitted from the cluster periphery. In contrast, the linear behavior observed for q beyond +10 monoatomic fragments, varies under even a minor change of the laser irradiation conditions. For this reason the mechanism involves in this case seems to rise from an other expansion process. The experiment on laser pulse duration influence as well as the simulations results point out an electron confinement process which leads to a free electron cloud formation inside the cluster. This electron cloud absorbs laser energy and participates to electrons-ions collisionnal ionization. This electron cloud could reach the resonance condition with the laser pulse intensity maximum which allows electrons to absorb a huge laser energy and lead to the greatest explosion.

4 Conclusion

We have experimentally demonstrated the presence of two explosion regimes for irradiated lead clusters. Using a simple time of flight mass spectrometer we have performed ionic mono atomic fragments analysis, which allows us to determine fragments kinetic energy. This fragments kinetic energy varies with the fragments charge state detected and also with the ultra short laser pulse parameters. We have also observed a quadratic dependence on charge state for Pb^{q+} with q below 9, independent on the field intensity in the range we run experiments and also independent on the pulse duration for a constant laser field intensity. This kinetic energy fragment behavior is interpreted as a signature that mono atomic ions are ejected from the cluster periphery by Coulomb repulsion at the beginning of the laser pulse. Indeed for ion charge state below 5 it is closely connected to the cluster radius in expansion. The second explosion regime is characterized by a linear dependence on fragments charge state for Pb^{q+} with q beyond +10. In this charge state region the linear kinetic energy dependence allows us to assign the initial kinetic energy of such ions to come from an important hydrodynamic pressure present inside the cluster. Indeed it has been shown that for all cluster size ranging from Pb_{20} to Pb_{2000} it does exist a sudden increase of the cluster energy absorbed under laser pulse duration conditions beyond 400 fs. Our experiment on laser pulse duration influence reveals a free electron cloud formation inside the cluster. When this electrons cloud reaches the resonance with the laser it is responsible for raising the hydrodynamic pressure in the cluster. These observations have been fully interpreted using the nanoplasma model developed by Ditmire and adapted here to metallic clusters. Briefly, first ionizations occur at the beginning of the laser pulse and generate a free electron cloud maintained by ions coulomb attraction inside the cluster. Electrons close to cluster surface leave the cluster, as a consequence the cluster presents a charge defect and some weakly charged ions are ejected. Moreover the free electrons cloud is involved in collisionnal ionizations and cluster heating. Indeed when the electrons cloud oscillation frequency allows a resonance with the laser frequency, the intra cluster electric field is increased and permits to obtain ionic fragments with the highest charge states. The so-formed hot plasma expands by hydrodynamic pressure effect.

As far as the metallic character of such clusters is concerned, it is revealed by a free electron cloud pre-existing in the initial cluster. This cloud could influence the effect of the first resonance described in the nano-plasma model. Nevertheless as the major effect is due to the second resonance when a large number of electrons are involved, the metallic character does not influence significantly the observed phenomena.

We have widely used the nano-plasma model abilities to have access to a qualitative interpretation of our results obtained in the feature A resolved part of our spectra. Nevertheless some theoretical efforts are needed in order to determine kinetic energy and charge state of fragments produced during the irradiation of a given cluster size distribution. Such a calculation should predict the emission of very high kinetic energy ions present in spectrum feature B and also the inner shell recombination phenomena suggested in the spectrum photon signal.

References

1. A. McPherson, B.D. Thompson, A.B. Borisov, K. Boyer, C.K. Rhodes, Nature **370**, 631 (1994)
2. A. McPherson, T.S. Luck, B.D. Thompson, A.B. Borisov, O.B. Shiryaev, X. Chen, K. Boyer, Phys. Rev. Lett. **72**, 1810 (1994)
3. J. Purnell, E.M. Snyder, S. Wei, A.W. Castelman Jr, Chem. Phys. Lett. **229**, 333 (1994)
4. C. Wülker, W. Theobald, D. Ouw, F.P. Schäfer, B.N. Chichkov, Opt. Commun. **112**, 21 (1994)
5. M. Lezius, S. Dobosz, D. Normand, M. Schmidt, Phys. Rev. Lett. **80**, 261 (1998)
6. T. Ditmire, J.W.G. Tisch, E. Springate, M.B. Mason, N. Hay, R.A. Smith, J. Marangos, M.H.R. Hutchinson, Nature **386**, 54 (1997)
7. Y.L. Shao, T. Ditmire, J.W.G. Tisch, E. Springate, J.P. Marangos, M.H.R. Hutchinson, Phys. Rev. Lett. **77**, 3343 (1996)
8. L.F. DiMauro, P. Agostini, Adv. At. Mol. Phys. **35**, 79 (1995)
9. C. Cornaggia, M. Schmidt, D. Normand, J. Phys B: At. Mol. Opt. Phys. **27**, L123 (1994)
10. C. Rose-Petruck, K.J. Schafer, K.R. Wilson, C.P.J. Barty, Phys. Rev. A **55**, 1182 (1997)
11. B.P. Thompson, A. McPherson, K. Boyer, C.K. Rhodes, J. Phys. B **27**, 4391 (1994)
12. T. Ditmire, T. Donelly, A.M. Rubenchik, R.W. Falcone, M.D. Perry, Phys. Rev. A **53**, 3379 (1996)
13. C. Bréchignac, P. Cahuzac, N. Kebaili, J. Leygnier, A. Sarfati, Phys. Rev. Lett. **68**, 3916 (1992)
14. C. Bréchignac, P. Cahuzac, N. Kebaili, J. Leygnier, A. Sarfati, Phys. Rev. Lett. **70**, 2036 (1993)
15. R. Schlipper, R. Kushe, B.v. Issendorff, H. Haberland, Phys. Rev. Lett. **80**, 1194 (1998)
16. B. Lang, A. Vierheilig, H. Buchenau, G. Gerber, Z. Phys. D **40**, 1 (1997)
17. T. Döppner, S. Teuber, M. Schumacher, K.H. Meiwes-Broer, Int. J. Mass Spec. **192**, 387 (1999)
18. L. Köller, M. Schumcher, J. Köhn, S. Teuber, J. Tiggesbäumker, K.H. Meiwes-Broer, Phys. Rev. Lett. **82**, 3783 (1999)
19. S. Teuber, T. Döppner, M. Schumacher, J. Tiggesbäumker, K.H. Meiwes-Broer, Aust. J. Phys. **52**, 555 (1999)
20. F. Calvayrac, A. Domps, P.-G. Reinhard, E. Suraud, C.A. Ulrich, Eur. Phys. J. D **4**, 207 (1998)
21. T. Döppner, S. Teuber, M. Schumacher, J. Tiggesbäumker, K.H. Meiwes-Broer, Appl. Phys. B **71**, 357 (2000)
22. V. Boutou, M.A. Lebeault-Dorget, A.R. Allouche, C. Bordas, J. Chevaleyre, Z. Phys. D **40**, 448 (1997)
23. M. Lezius, S. Dobosz, D. Normand, M. Schmidt, J. Phys. B **30**, L251 (1997)
24. N.W. Ashcroft, N.D. Mermin, *Solid State Physics* (Holt, Rinehart and Winston, New York, 1976)
25. S. Bertier, *Optique des milieux composites* (Polytechnica, Paris, 1993)
26. J. Zweiback, T. Ditmire, M.D. Perry, Phys. Rev. A **59**, R3166 (1999)